served in endometrial hyperplasia. In contrast, ERs were assumed to be reduced in endometrial carcinoma with accelerated glucose metabolism measured by FDG-PET. Here, we report two cases of endometrial hyperplasia on tamoxifen treatment, which had a distinctive accumulation pattern of FDG and FES on PET.

Materials and methods

PET and MRI procedure

FES was synthesized according to the method of Kiesewetter et al. [10] with modifications as reported by Mori et al. [11]. It is an automated production method for FES using TRACERlab MX_{FDG} which is a cassette-type automatic FDG synthesizer (GE Medical Systems, Milwaukee, WI, USA). The detailed process of pharmacologic synthesis is described in their literature.

Patients fasted for at least 4h before receiving an intravenous injection of 185MBq of tracer. FDG- and FES-PET scans were performed within a 1-week interval using a whole-body PET scanner (ADVANCE; GE Medical System) with a transaxial spatial resolution of 5mm at full width at half maximum in a two-dimensional acquisition mode. Attenuation was corrected by standard transmission scanning with $^{68}Ge/^{68}Ga$ sources. The PET scans were performed in seven bed positions that started at 50min following the injection of FDG and FES. The acquisition data were reconstructed using an iterative reconstruction method (subsets 14, number of iterations 2).

The pelvic MRI was obtained within 1 week prior to the PET scan using a 1.5-T system (Signa, GE Medical Systems). The MRI examination included T1- and T2-weighted images and fat-suppressed T1-weighted image with gadolinium (Gd) contrast enhancement.

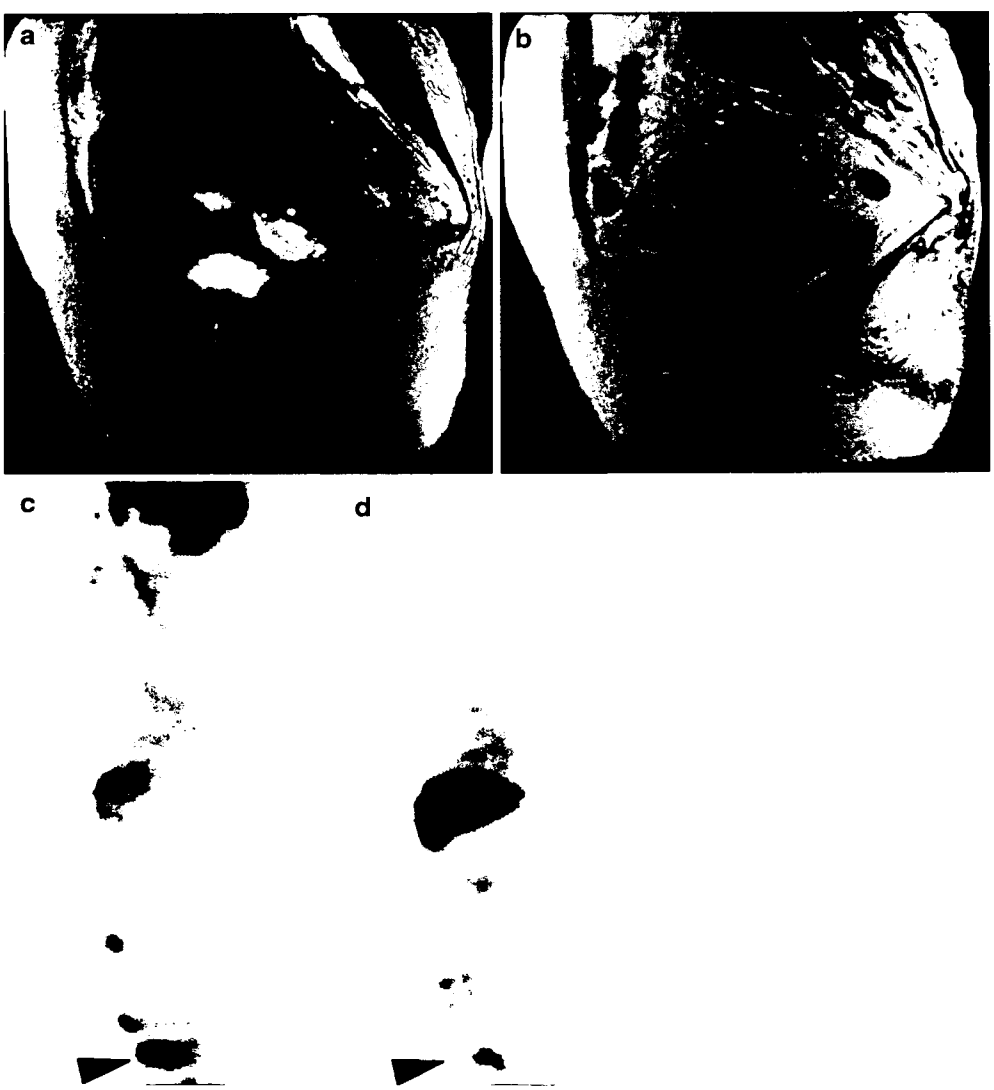

Fig. 1 Sagittal T2- (**a**) and gadolinium (Gd)-enhanced T1- (**b**) weighted images showing endometrial thickening and suspicion of cervical interstitial invasion. Sagittal positron emission tomography (PET) images with 2-[^{18}F]fluoro-2-deoxy-D-glucose (FDG, **c**) and 16α-[^{18}F]fluoro-17β-estradiol (FES, **d**) showing no abnormal uptake in the endometrial lesion. *Arrowheads* show tracer accumulation in the bladder

Case reports

Case 1

An 80-year-old woman was referred to our hospital for the diagnosis and treatment of an endometrial lesion. Following surgery for right breast cancer about 2 years earlier, she had been taking tamoxifen. The smear cytology of the patient was positive. The pelvic MRI suggested endometrial thickening with cervical interstitial invasion on T2- and Gd-enhanced T1-weighted images (Fig. 1a, b). Stage IIb endometrial carcinoma was considered from the MRI findings on the basis of the International Federation of Gynecology and Obstetrics (FIGO) classification. However, the FDG-PET image showed no abnormal uptake of FDG in the endometrial lesion, suggesting negative for malignancy (Fig. 1c). The FES-PET image similarly showed no abnormal uptake of FES (Fig. 1d). Taking medicine on the day of each PET scan had been prohibited. The postoperative histopathologic examination revealed that the lesion was atypical endometrial hyperplasia.

Case 2

A 79-year-old woman was hospitalized for the evaluation of a uterine enlargement. She had been taking tamoxifen for 7 years following surgery for breast cancer. The smear cytology of the patient was negative. The T2-weighted MRI image showed uterine enlargement with severe endometrial thickening and adenomyosis (Fig. 2a). The Gd-enhanced T1-weighted MR image suggested

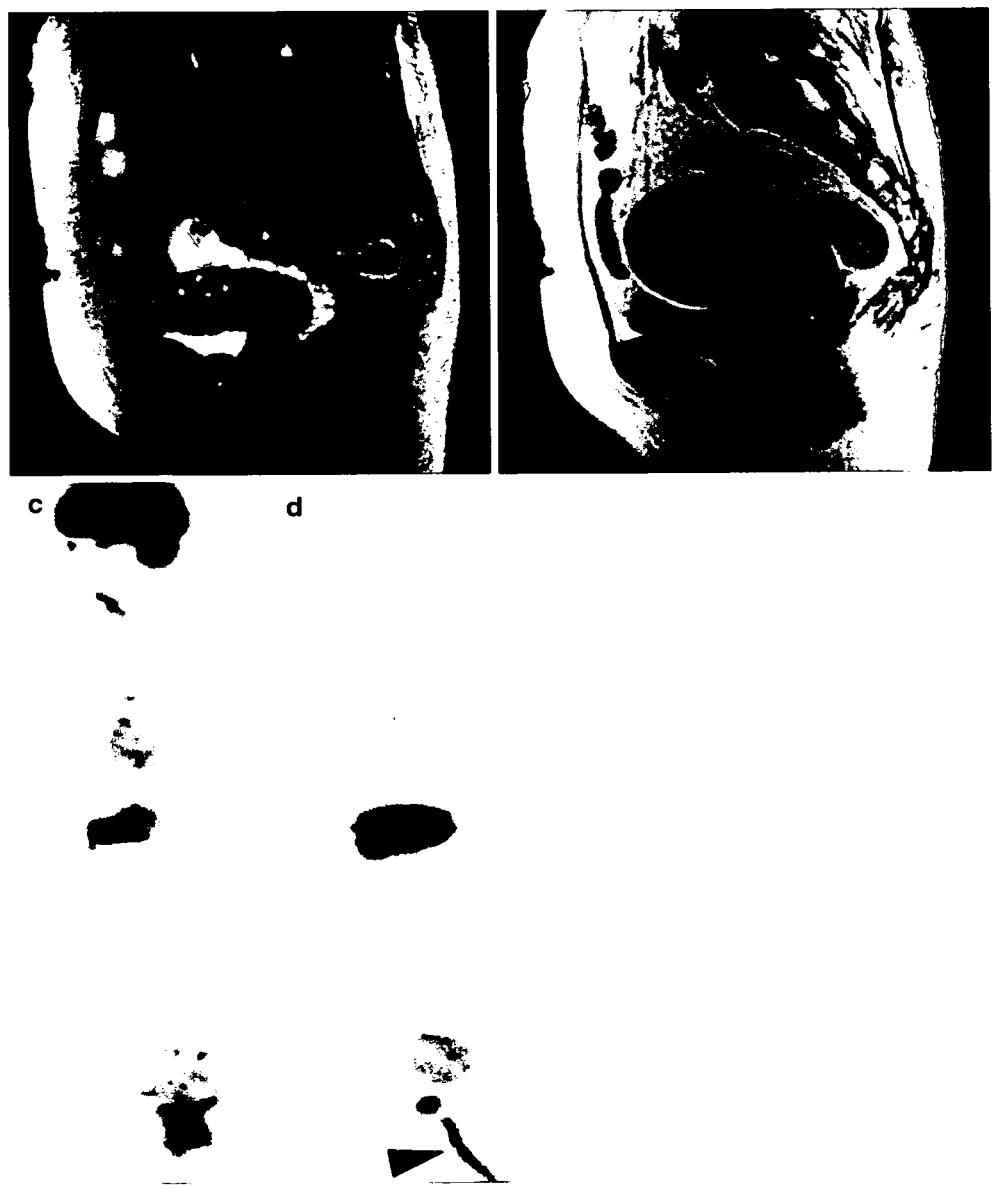

Fig. 2 T2-weighted magnetic resonance imaging (MRI) showing uterine enlargement with severe endometrial thickening and adenomyosis (**a**). Gd-enhanced T1-weighted MRI image suggesting muscular invasion (**b**). However, PET images with FDG (**c**) and FES (**d**) showing no abnormal uptake. *Arrowhead* showing tracer accumulation in drainage tube

muscular invasion (Fig. 2b). She was suspected of having stage Ib endometrial carcinoma from the MRI findings. FDG- and FES-PET showed no abnormal uptake (Fig. 2c, d). As in case 1, taking medicine on the day of each PET scan had been prohibited. The postoperative histopathologic examination revealed that the lesion was mild endometrial hyperplasia.

Discussion

Recent investigations have focused on the ER expression of endometrial lesions and the mechanism of estrogen and selective estrogen receptor modulators (SERMs) in endometrial carcinogenesis, which still remains to be clarified [12]. Tamoxifen is one of the SERMs whose divergent estrogen agonist and antagonist effects have been recognized in different target organs. It acts as an estrogen antagonist in the mammary gland but as an estrogen agonist in the uterine endometrium. The association between endometrial carcinoma and tamoxifen was first recognized in 1985 when three cases of endometrial carcinoma were described in women who had been treated with tamoxifen for breast cancer [13]. Another estrogen-dependent gynecologic abnormality is endometrial hyperplasia, which is usually a benign lesion but is also considered to represent the incipient stage of endometrial carcinoma. The differential diagnosis between endometrial carcinoma and hyperplasia is sometimes difficult in smear cytology, pelvic MRI, and even in endometrial curettage. Whole endometrial curettage under general anesthesia, which is very invasive, may be needed additionally. A noninvasive diagnosis of endometrial hyperplasia is considered to be very valuable for preserving women's reproductivity. Premenopausal women noninvasively diagnosed with endometrial hyperplasia, who have yet to complete their family, would be able to receive conservative treatment using medroxyprogesterone acetate (MPA), etc.

FES is an ER-imaging tracer and FES-PET is well established in patients with ER-positive breast cancer for its diagnosis, staging, and follow-up [3–8]. ER exists in two main forms, namely, ERα and ERβ, with Yoo et al. [14] reporting that the binding affinity of FES is 6.3-fold higher for ERα than for ERβ. In addition, the recent investigation of Tsuchida et al. [15] demonstrated that FES-PET could describe the change of endometrial ERα concentration relative to menstrual cycle in normal volunteers. On the basis of these studies, we have been using FES-PET as an ERα imaging modality not only for breast cancer but also for gynecologic diseases. We recently reported that patients with endometrial carcinoma showed a significantly higher accumulation of

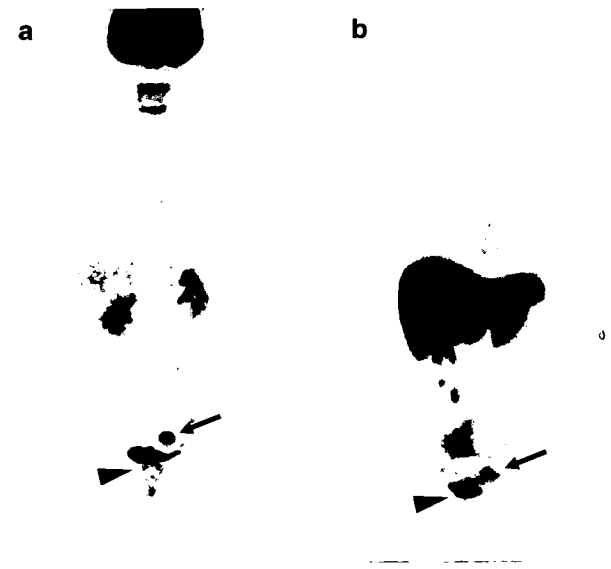

Fig. 3 A 40-year-old patient with endometrial carcinoma. Maximum intensity projection images of FDG-PET (**a**) and FES-PET (**b**) showing a significantly higher accumulation of FDG than FES in the primary tumor (*arrows*). Standardized uptake values (SUVs) were 15.2 (**a**) and 2.5 (**b**). *Arrowheads* showing tracer accumulation in the bladder

FDG than FES in the primary tumors, and those patients with endometrial hyperplasia showed a significantly higher FES uptake than FDG [9] (Figs. 3–4). Using the opposite tracer accumulation pattern a combined FES- and FDG-PET scan was considered to be a useful diagnostic tool which provided supplementary information on the differential diagnosis of endometrial tumors. Nevertheless, in both of the present cases on tamoxifen treatment, FDG- and FES-PET showed no abnormal accumulation in endometrial hyperplasia. These results indicate that in endometrial hyperplasia, glucose metabolism via glucose transporter 1 would not increase as much as in endometrial carcinoma [16], and that tamoxifen may reduce ERα expression or compete with FES for binding ERα. The assumption that tamoxifen may reduce ERα expression is consistent with the findings of some earlier reports [17, 18]; however, the biggest contributor to negative FES uptake of endometrial hyperplasia seemed to be binding to ERs of tamoxifen or its metabolites [19]. Tamoxifen half-life was reported to be about 7 days following chronic dosing in patients with breast cancer [20]. The present patients who had been taking tamoxifen for several years should have stopped taking it at least several weeks prior to the day of the FES-PET scan. On the other hand, an agent such as MPA or aromatase inhibitor, which does not target ERs, has no direct effect on the evaluation of ER density using FES-PET [21].

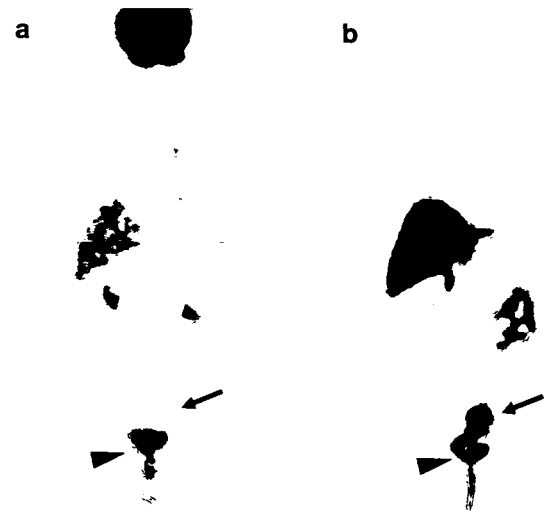

Fig. 4 A 67-year-old patient with endometrial hyperplasia. Coronal PET images with FDG (**a**) and FES (**b**) showing a significantly higher FES uptake than FDG in the primary tumors (*arrows*). SUVs were 2.3 (**a**) and 11.0 (**b**). *Arrowheads* showing tracer accumulation in the bladder

FES-PET enables us to evaluate the ERα expression of endometrium noninvasively, whereas the evaluation of ER expression using FES-PET requires careful attention to the influence of hormonal therapy because tamoxifen greatly affects FES accumulation of even endometrial hyperplasia, which should be an FES-avid lesion.

References

1. Kurman RJ, Kaminski PF, Norris HJ. The behavior of endometrial hyperplasia: a long-term study of "untreated" hyperplasia in 170 patients. Cancer 1985;56:403–12.
2. Havrilesky LJ, Kulasingam SL, Matchar DB, Myers ER. FDG-PET for management of cervical and ovarian cancer. Gynecol Oncol 2005;97:183–91.
3. Mintun MA, Welch MJ, Siegel BA, Mathias CJ, Brodack JW, McGuire AH, et al. Breast cancer: PET imaging of estrogen receptors. Radiology 1988;169:45–8.
4. McGuire AH, Dehdashti F, Siegel BA, Lyss AP, Brodack JW, Mathias CJ, et al. Positron tomographic assessment of 16α-[^{18}F]fluoro-17β-estradiol uptake in metastatic breast carcinoma. J Nucl Med 1991;32:1526–31.
5. Dehdashti F, Mortimer JE, Siegel BA, Griffeth LK, Bonasera TJ, Fusselman MJ, et al. Positron tomographic assessment of estrogen receptors in breast cancer: comparison with FDG-PET and in vitro receptor assays. J Nucl Med 1995;36:1766–74.
6. Dehdashti F, Flanagan FL, Mortimer JE, Katzenellenbogen JA, Welch MJ, Siegel BA. Positron emission tomographic assessment of "metabolic flare" to predict response of metastatic breast cancer to antiestrogen therapy. Eur J Nucl Med 1999;26:51–6.
7. Mortimer JE, Dehdashti F, Siegel BA, Trinkaus K, Katzenellenbogen JA, Welch MJ. Metabolic flare: indicator of hormone responsiveness in advanced breast cancer. J Clin Oncol 2001;19:2797–803.
8. Linden HM, Stekhova SA, Link JM, Gralow JR, Livingston RB, Ellis GK, et al. Quantitative fluoroestradiol positron emission tomography imaging predicts response to endocrine treatment in breast cancer. J Clin Oncol 2006;24:2793–9.
9. Tsujikawa T, Okazawa H, Yoshida Y, Mori T, Kobayashi M, Tsuchida T, et al. Differential diagnosis of endometrial hyperplasia and cancer using combined 18F-FES and 18F-FDG PET (abstract). J Nucl Med 2007;48 Suppl 2:386P.
10. Kiesewetter DO, Kilbourn MR, Landvatter SW, Heiman DF, Katzenellenbogen JA, Welch MJ. Preparation of four fluorine-18-labeled estrogens and their selective uptakes in target tissues of immature rats. J Nucl Med 1984;25:1212–21.
11. Mori T, Kasamatsu S, Mosdzianowski C, Welch MJ, Yonekura Y, Fujibayashi Y. Automatic synthesis of 16α-[^{18}F]fluoro-17β-estradiol using a cassette-type [^{18}F]fluorodeoxyglucose synthesizer. Nucl Med Biol 2006;33:281–6.
12. Hu K, Zhong G, He F. Expression of estrogen receptors ERα and ERβ in endometrial hyperplasia and adenocarcinoma. Int J Gynecol Cancer 2005;15:537–41.
13. Killackey MA, Hakes TB, Pierce VK. Endometrial adenocarcinoma in breast cancer patients receiving antiestrogens. Cancer Treat Rep 1985;69:237–8.
14. Yoo J, Dence CS, Sharp TL, Katzenellenbogen JA, Welch MJ. Synthesis of an estrogen receptor β-selective radioligand: 5-[^{18}F]fluoro-(2R*,3S*)-2,3-bis(4-hydroxyphehyl) pentanenitrile and comparison of in vivo distribution with 16α-[^{18}F]fluoro-17β-estradiol. J Med Chem 2005;48:6366–78.
15. Tsuchida T, Okazawa H, Mori T, Kobayashi M, Yoshida Y, Fujibayashi Y, et al. In vivo imaging of estrogen receptor concentration in the endometrium and myometrium using FES PET: influence of menstrual cycle and endogenous estrogen level. Nucl Med Biol 2007;34:205–10.
16. Wang BY, Kalir T, Sabo E, Sherman DE, Cohen C, Burstein DE. Immunohistochemical staining of GLUT1 in benign, hyperplastic, and malignant endometrial epithelia. Cancer 2000;88:2774–81.
17. Cohen I, Beyth Y, Altaras MM, Shapira J, Tepper R, Cardoba M, et al. Estrogen and progesterone receptor expression in postmenopausal tamoxifen-exposed endometrial pathologies. Gynecol Oncol 1997;67:8–15.
18. Wilder JL, Shajahan S, Khattar NH, Wilder DM, Yin J, Rushing RS, et al. Tamoxifen-associated malignant endometrial tumors: pathologic features and expression of hormone receptors estrogen-α, estrogen-β and progesterone: a case controlled study. Gynecol Oncol 2004;92:553–8.
19. Furr BJ, Nicholson RI. The pharmacology and clinical uses of tamoxifen. Pharmacol Ther 1984;25:127–205.
20. Fabian C, Sternson L, El-Serafi M, Cain L, Hearne E. Clinical pharmacology of tamoxifen in patients with breast cancer: correlation with clinical data. Cancer 1981;48:876–82.
21. Yoshida Y, Kurokawa T, Sawamura Y, Shinagawa A, Okazawa H, Fujibayashi Y, et al. The positron emission tomography with F18 17β-estradiol has the potential to benefit diagnosis and treatment of endometrial cancer. Gynecol Oncol 2007;104:764–6.

資料(14)

Ann Nucl Med (2007) 21:375–378
DOI 10.1007/s12149-007-0037-8

CASE REPORT

A ^{18}F-FDG-positive, ^{67}Ga-negative, and transferrin receptor expression-negative patient with diffuse large B-cell lymphoma

Tetsuya Tsujikawa · Hidehiko Okazawa
Tatsuro Tsuchida · Yoshiki Demura · Yoshiaki Imamura
Yasuhisa Fujibayashi

Received: 19 January 2007 / Accepted: 10 April 2007

Abstract We recently experienced a case with uveitis suffering from fever of unknown origin suspected of being caused by sarcoidosis. Chest computed tomography showed right supraclavicular, bilateral mediastinal, and right hilar lymphadenopathy, and intensive abnormal uptake of 2-[^{18}F]fluoro-2-deoxy-D-glucose (^{18}F-FDG) was observed on positron emission tomography with ^{18}F-FDG (FDG-PET). On the other hand, ^{67}Ga scintigraphy showed almost no abnormal findings. Histopathological examination revealed the lesion to be a diffuse large B-cell lymphoma (DLBCL), namely, an aggressive non-Hodgkin lymphoma from a right supraclavicular lymph node biopsy specimen. Additional immunohistochemical analysis showed the negative expression of transferrin receptor (TfR) on the formalin-fixed paraffin-embedded specimen. Although DLBCL is generally considered to be a ^{67}Ga-avid tumor, it does not always have a large number of TfRs and that leads to a discrepancy between the ^{67}Ga scintigraphy and FDG-PET findings. FDG-PET should be more appropriate for the initial staging of DLBCL than ^{67}Ga scintigraphy, whereas ^{67}Ga scintigraphy might be able to provide additional information including prognostic factors and to support strategies that target TfR for cancer therapy.

Keywords Diffuse large B-cell lymphoma · ^{67}Ga scintigraphy · Transferrin receptor · FDG-PET

T. Tsujikawa (✉) · H. Okazawa · Y. Fujibayashi
Biomedical Imaging Research Center, University of Fukui, 23-3 Matsuoka-Shimoaizuki, Eiheiji-cho, Fukui 910-1193, Japan
e-mail: awaji@u-fukui.ac.jp

T. Tsuchida
Department of Radiology, University of Fukui, Fukui, Japan

Y. Demura
Third Department of Internal Medicine, University of Fukui, Fukui, Japan

Y. Imamura
Department of Pathology, University of Fukui, Fukui, Japan

Introduction

^{67}Ga and 2-[^{18}F]fluoro-2-deoxy-D-glucose (^{18}F-FDG) are tumor viability indicators and ^{67}Ga scintigraphy and positron emission tomography with ^{18}F-FDG (FDG-PET) have been widely used for the management of lymphomas. The tissue uptake of tracers by malignant tumors is based on different mechanisms. Malignant cells accumulate ^{67}Ga mainly through an intracellular transferrin (Tf)-related transport mechanism via a ^{67}Ga–Tf complex [1, 2]. Transferrin receptor (TfR) is a key cell surface molecule that regulates uptake of iron-bound Tf by receptor-mediated endocytosis, and an overexpression of TfR is assumed to be a common feature of malignant tumors. Kiratli et al. [3] showed that rapidly proliferating tumors with a high level of DNA synthesis have high TfR expression for increasing iron uptake and enhance ^{67}Ga uptake in a flow cytometric analysis in patients with lymphoma. On the other hand, ^{18}F-FDG is a glucose analogue, which reflects the activity of glucose transport proteins and the intracellular phosphorylation by hexokinase [4, 5]. ^{67}Ga scintigraphy and FDG-PET have been useful for the initial staging and post-therapeutic follow-up of lymphomas [6].

We report a case of diffuse large B-cell lymphoma (DLBCL), which showed a discrepancy between the ^{67}Ga scintigraphy and FDG-PET findings, and discuss the advantages of each examination for tumor imaging.

Ann Nucl Med (2007) 21:375–378

Fig. 1 Chest computed tomography (CT) images showing right supraclavicular, bilateral mediastinal, and right hilar lymphadenopathy

Methods

The FDG-PET scan was performed with a GE ADVANCE (GE Medical Systems, Milwaukee, WI, USA). Before tracer administration, at least a 4-h fasting was required and emission data were collected for 2 min per frame using 2D acquisition at 50 min after the injection of 185 MBq ^{18}F-FDG. Transmission scan was obtained before emission scan using 68Ge/68Ga rod source for attenuation correction. The acquired data were reconstructed by the iterative reconstruction method selecting 14 subsets, 2 iterations, and 128 × 128 matrix.

^{67}Ga scintigraphy was performed at 72 h after the injection of 111 MBq ^{67}Ga-citrate. Imaging was obtained by an E-CAM (Siemens Medical Systems, Hoffman Estates, IL, USA) with medium-energy and a general-purpose collimator. Whole-body imaging was performed with both anterior and posterior view images.

Case report

A 69-year-old man suffering from fever of unknown origin was referred to our hospital. He had been treated for uveitis and received left vitrectomy because of left vitreous hemorrhage. On admission, his right supraclavicular lymph nodes (10 mm × 2, elastic hard) were palpable. He underwent chest computed tomography (CT), ^{67}Ga scintigraphy, and whole-body FDG-PET scan. Chest CT showed right supraclavicular, bilateral mediastinal, and right hilar lymphadenopathy (Fig. 1), and his physician considered him to have sarcoidosis on the basis of the clinical course (uveitis and lymphadenopathy). Intensive ^{18}F-FDG accumulations of the lymphadenopathy and an incidental nodular uptake of ^{18}F-FDG in the left pelvis were observed on FDG-PET (Fig. 2). In contrast, ^{67}Ga scintigraphy showed almost no abnormal findings except for slightly increased left hilar ^{67}Ga uptake (Fig. 3). The left hilar accumulation of ^{67}Ga was regarded as a non-specific physiological one because of the absence of left hilar lymphadenopathy on chest CT. Histopathological examination from a right

Fig. 2 Fluoro-2-deoxy-D-glucose (FDG) positron emission tomography image showing intensive ^{18}F-FDG accumulations of the lymphadenopathy and an incidental nodular uptake of ^{18}F-FDG in left pelvis

Fig. 3 ^{67}Ga scintigraphy was almost normal. Slightly increased left hilar accumulation was regarded as a non-specific physiological one because of the absence of left hilar lymphadenopathy detected on chest CT

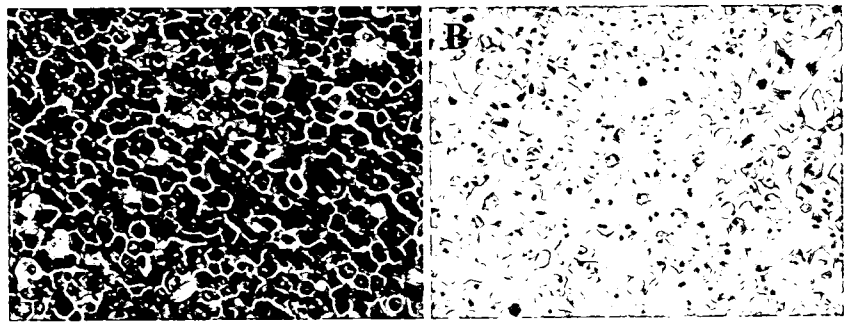

Fig. 4 a Histological image of right supraclavicular lymph node showing the typical appearance of diffuse large B-cell lymphoma on hematoxylin–eosin. The tumor cells show diffuse growth pattern and they have large vesicular nuclei with prominent eosinophilic nucleoli. b Immunohistochemical image showing negative expression of transferrin receptor

supraclavicular lymph node biopsy specimen revealed the lesion to be DLBCL (Fig. 4a). To resolve the difference between ^{67}Ga scintigraphy and FDG-PET findings, additional immunohistochemical analysis was done, and showed negative expression of TfR on the formalin-fixed paraffin-embedded specimen (Fig. 4b). Furthermore, pelvic MRI after FDG-PET revealed the nodular ^{18}F-FDG uptake in the left pelvis to be an involvement by DLBCL of the left ischium, and the patient was finally diagnosed as having DLBCL stage IV.

Discussion

It should be emphasized that there was a discrepancy between ^{67}Ga and ^{18}F-FDG uptake of DLBCL without TfR expression. This result is consistent with previous reports in which when the tumor tissue was positive for TfR, ^{67}Ga was positive, and a negative ^{67}Ga scan correlated with the absence of TfR in the biopsied tissue [7, 8]. Some researchers concluded that TfR expression on a tumor correlates with its grade [9, 10]. DLBCL is classified as an aggressive non-Hodgkin lymphoma (NHL), which is generally considered to be a ^{67}Ga-avid tumor. In the literature, aggressive lymphomas such as DLBCL were reported to contain about 20% TfR positive lymphocytes in biopsy material from nodes involved by lymphoma [11, 12]. However, immunohistochemical analysis in our case showed negative TfR expression, and ^{67}Ga accumulation was low. Nejmeddine et al. [13] suggested that there were three factors influencing ^{67}Ga uptake in NHL: histology, TfR expression, and the presence of a large cells component. Although DLBCL generally has all these factors, TfR expression was negative in our case. Our case revealed that DLBCL does not always have a large number of TfRs, accounting for the discrepancy between the ^{67}Ga scintigraphy and FDG-PET findings.

At the same time, it should be noted that ^{67}Ga is brought to tumors mainly by Tf via a ^{67}Ga-Tf complex, whereas it can be partially translocated to lactoferrin (LF) and incorporated into tumor cells via a ^{67}Ga–LF complex [1]. This kind of TfR-independent process is considered to occur both in vitro and in vivo [2]. Furthermore, ^{67}Ga accumulation in tumors is mediated by other factors such as anaerobic tumor metabolism, increased tumor perfusion, and vascular permeability. ^{67}Ga accumulation may require a set of circumstances to be fulfilled, whereas hypermetabolism as evidenced by increased glycolysis by the tumor cells is sufficient for ^{18}F-FDG uptake [14].

The recent investigation of O'Donnell et al. [15] showed the relationship between TfR expression and c-Myc which is one of the most frequently dysregulated proteins and stimulates proliferation and growth by activating thousands of target genes in malignancies. They revealed that TfR expression is activated by c-Myc in B-cell lymphoma and TfR is required for c-Myc-mediated cellular proliferation: after all, TfR inhibition decreases cellular proliferation and results in G1 arrest. In the light of their report, we might be able to use ^{67}Ga scintigraphy for prognostic prediction of patients with lymphoma. The patient in this case actually has not yet relapsed about half a year after he attained a complete response to chemotherapy.

In contrast to ^{67}Ga scintigraphy, FDG-PET clearly delineated all lesions of DLBCL before treatment in our case. Kostakoglu et al. [16] showed the superiority of FDG-PET to ^{67}Ga scintigraphy by higher tumor-to-background ratio and higher site and patient sensitivity of FDG-PET than ^{67}Ga scintigraphy in 51 patients with untreated lymphoma. In fact, FDG-PET has been expected to take the place of ^{67}Ga scintigraphy for tumor imaging because of its higher resolution and diagnostic accuracy during the past 10 years [17, 18]. Moreover, integrated PET and CT with FDG (FDG-PET/CT) has appeared as a new imaging modality, providing anatomic and metabolic information. FDG-PET/CT allows more accurate spatial localization of abnormal ^{18}F-FDG uptake than PET alone, and it has become the most preferable initial staging tool for patients with NHL [19]. As for ^{67}Ga scintigraphy, SPECT/CT scan is also

used for increasing diagnostic accuracy in the clinical management of lymphoma. ^{67}Ga-SPECT/CT is reported to provide additional anatomical information over SPECT alone especially in the abdomen or pelvis [20]. Furthermore, a monoclonal TfR antibody, A 24, was shown to induce apoptosis in T-lymphocytes from patients with CD71-positive T-cell leukemias [21]. ^{67}Ga scan including SPECT/CT might be able to support strategies that target TfR for cancer therapy.

Transferrin receptor expression on malignant cells is considered to greatly influence ^{67}Ga accumulation in patients with DLBCL. FDG-PET or PET/CT might be more appropriate for the initial staging of DLBCL than ^{67}Ga scintigraphy. However, ^{67}Ga scan might be able to provide additional important information including prognostic prediction and support strategies that target TfR for cancer therapy.

References

1. Weiner RE. The mechanism of ^{67}Ga localization in malignant disease. Nucl Med Biol 1996;23:745–51.
2. Luttropp CA, Jackson JA, Jones BJ, Sohn MH, Lynch RE, Morton KA. Uptake of gallium-67 in transfected cells and tumors absent or enriched in the transferrin receptor. J Nucl Med 1998;39:1405–11.
3. Kiratli PO, Canpinar H, Ruacan S, Kansu E. Correlation of flow cytometric parameters and transferrin receptors with gallium-67 scintigraphic images in lymphoma patients. Nucl Med Commun 2000;21:925–31.
4. Chung JK, Lee YJ, Kim C, Choi SR, Kim M, Lee K, et al. Mechanisms related to [^{18}F]fluorodeoxyglucose uptake of human colon cancers transplanted in nude mice. J Nucl Med 1999;40:339–46.
5. Higashi K, Ueda Y, Sakurai A, Wang XM, Xu L, Murakami M, et al. Correlation of Glut-1 glucose transporter expression with [^{18}F]FDG uptake in non-small cell lung cancer. Eur J Nucl Med 2000;27:1778–85.
6. Bar-Shalom R, Mor M, Yefremov N, Goldsmith SJ. The value of Ga-67 scintigraphy and F-18 fluorodeoxyglucose positron emission tomography in staging and monitoring the response of lymphoma to treatment. Semin Nucl Med 2001;31: 177–90.
7. Feremans W, Bujan W, Neve P, Delville JP, Schandene L. CD71 phenotype and the value of gallium imaging in lymphomas. Am J Hematol 1991;36:215–6.
8. Tsuchiya Y, Nakao A, Komatsu T, Yamamoto M, Shimokata K. Relationship between gallium 67 citrate scanning and transferrin receptor expression in lung diseases. Chest 1992; 102:530–4.
9. Medeiros LJ, Picker LJ, Horning SJ, Warnke RA. Transferrin receptor expression by non-Hodgkin's lymphomas: correlation with morphologic grade and survival. Cancer 1988;61: 1844–51.
10. Das Gupta A, Shah VI. Correlation of transferrin receptor expression with histologic grade and immunophenotype in chronic lymphocytic leukemia and non-Hodgkin's lymphoma. Hematol Pathol 1990;4:37–41.
11. Gallamini A, Biggi A, Fruttero A, Pugno F, Cavallero G, Pregno P, et al. Revisiting the prognostic role of gallium scintigraphy in low-grade non-Hodgkin's lymphoma. Eur J Nucl Med 1997;24:1499–506.
12. Habeshaw JA, Lister TA, Stansfeld AG, Greaves MF. Correlation of transferrin receptor expression with histological class and outcome in non-Hodgkin lymphoma. Lancet 1983;1: 498–501.
13. Nejmeddine F, Raphael M, Martin A, Le Poux G, Moretti JL, Caillat-Vigneron N. ^{67}Ga scintigraphy in B-cell non-Hodgkin's lymphoma: correlation of ^{67}Ga uptake with histology and transferrin receptor expression. J Nucl Med 1999; 40:40–5.
14. Kostakoglu L, Goldsmith SJ. Lymphoma imaging: nuclear medicine. Cancer Treat Res 2006;131:363–412.
15. O'Donnell KA, Yu D, Zeller KI, Kim JW, Racke F, Thomas-Tikhonenko, et al. Activation of transferrin receptor 1 by c-Myc enhances cellular proliferation and tumorigenesis. Mol Cell Biol 2006;26:2373–86.
16. Kostakoglu L, Leonard JP, Kuji I, Coleman M, Vallabhajosula S, Goldsmith SJ. Comparison of fluorine-18 fluorodeoxyglucose positron emission tomography and Ga-67 scintigraphy in evaluation of lymphoma. Cancer 2002;94: 879–88.
17. Hoh CK, Glaspv J, Rosen P, Dahlbom M, Lee SJ, Kunkel L, et al. Whole-body FDG-PET imaging for staging of Hodgkin's disease and lymphoma. J Nucl Med 1997;38:343–8.
18. Moog F, Banerter M, Diederichs CG, Guhlmann A, Kotzerke J, Merkle E, et al. Lymphoma: role of whole-body 2-deoxy-2-[F-18]fluoro-D-glucose (FDG) PET in nodal staging. Radiology 1997;203:795–800.
19. Hicks RJ, Mac Manus MP, Seymour JF. Initial staging of lymphoma with positron emission tomography and computed tomography. Semin Nucl Med 2005;35:165–75.
20. Palumbo B, Sivolella S, Palumbo I, Liberati AM, Palumbo R. ^{67}Ga-SPECT/CT with a hybrid system in the clinical management of lymphoma. Eur J Nucl Med Mol Imaging 2005;32: 1011–7.
21. Moura IC, Centelles MN, Arcos-Fajardo M, Malheiros DM, Collawn JF, Cooper MD, et al. A neutralizing monoclonal antibody (mAb A24) directed against the transferrin receptor induces apoptosis of tumor T lymphocytes from ATL patients. Blood 2004;103:1838–45.

資料(15)

資料 15

Available online at www.sciencedirect.com

ScienceDirect

Nuclear Medicine and Biology 35 (2008) 171–176

NUCLEAR MEDICINE — AND — BIOLOGY

www.elsevier.com/locate/nucmedbio

Grading of brain glioma with 1-^{11}C-acetate PET: comparison with ^{18}F-FDG PET

Tatsuro Tsuchida[a,*], Hiroaki Takeuchi[b], Hidehiko Okazawa[c], Tetsuya Tsujikawa[c], Yasuhisa Fujibayashi[c]

[a]*Department of Radiology, Faculty of Medical Sciences, University of Fukui, Fukui 910-1193, Japan*
[b]*Department of Neurosurgery, Faculty of Medical Sciences, University of Fukui, Fukui 910-1193, Japan*
[c]*Biomedical Imaging Research Center, University of Fukui, Fukui 910-1193, Japan*

Received 27 August 2007; received in revised form 17 October 2007; accepted 7 November 2007

Abstract

The objective of this study is to reevaluate the clinical significance of 1-^{11}C-acetate (ACE) positron emission tomography (PET) in patients with brain glioma, in comparison with ^{18}F-fluorodeoxyglucose (FDG) PET.

Methods: Ten patients with histologically proven glioma were included in this study. They underwent PET examination with both FDG and ACE on separate days. For ACE PET, 20-min data acquisition was performed just after the administration of 740 MBq of ACE; 10–20-min data were used for the analysis. FDG PET data acquisition for 10 min started 60 min postinjection of 370 MBq of FDG, approximately. Both reconstructed images were converted to standardized uptake value (SUV) images for patient body weight and injected dose. Regions of interest were placed on the tumor and the contralateral cerebral cortex, and SUV and tumor-to-cortex ratio (T/C) were calculated; these values were compared between high- and low-grade gliomas.

Results: SUV and T/C of ACE PET showed significant difference (SUV: 2.63±0.46 vs. 1.85±0.56, P=.03; T/C: 2.36±0.63 vs. 1.14±0.36, P=.02). In contrast, FDG PET revealed no significant difference in SUV or T/C between high- and low-grade gliomas (SUV: 7.13±4.31 vs. 4.71±1.27, P=.31; T/C: 0.98±0.55 vs. 0.62±0.09, P=.22).

Conclusion: This preliminary study revealed that ACE PET is a promising tracer for the grading of brain glioma.

Keywords: 1-^{11}C-acetate; ^{18}F-FDG; Positron emission tomography; Glioma; Grading

1. Introduction

Positron emission tomography (PET) with ^{18}F-fluorodeoxyglucose (FDG) has been widely used for various kinds of neoplasm in differentiating between benign and malignant, staging, survey for recurrence and evaluating therapeutic effect [1]. The usefulness of FDG PET for brain tumors has been summarized previously [2]; however, localization of gliomas can be difficult because of high FDG uptake in the cerebral cortex, which results in high background activity [3] and limits the usefulness of FDG for radiation treatment planning [4]. Several kinds of radiopharmaceuticals, such as ^{11}C-methionine (MET), ^{18}F-fluoroethyl-L-tyrosine, methyl-^{11}C-choline (CHO) and 1-^{11}C-acetate (ACE) [5,6], have been proposed for the positive detection of brain tumors; among these, MET is well evaluated in terms of its ability to provide delineation from the normal cortex and differentiate between high-grade glioma and low-grade tumors compared to FDG [7,8] and/or ^{201}thallium chloride [9] and enable tumor differentiation [7–9]. Although similar results have also been reported for CHO [10], ACE showed limitations in differentiation in a previous report [11].

Yoshimoto et al. [12] reported in an in vitro study that 1-^{14}C-acetate accumulation correlates with ^{3}H-methyl thymidine incorporation; this indicates that the degree of ACE uptake represents cell proliferative activity and histologic grading.

In this context, we sought to reevaluate the clinical significance of ACE in terms of the histologic grading

* Corresponding author. Tel.: +81 776 61 3111x2335; fax: +81 776 61 8137.
E-mail address: tsucchy@u-fukui.ac.jp (T. Tsuchida).

0969-8051/$ – see front matter © 2008 Elsevier Inc. All rights reserved.
doi:10.1016/j.nucmedbio.2007.11.004

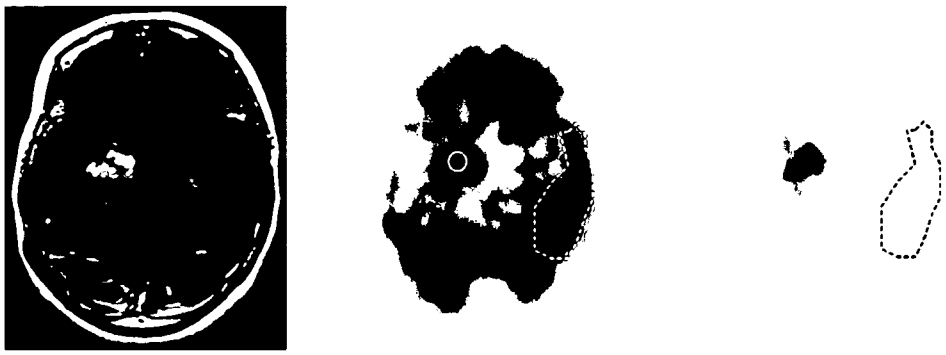

Fig. 1. Template of ROIs on FDG and ACE PET. ROIs were placed manually using MRI guidance.

of brain gliomas by comparing FDG both visually and quantitatively.

2. Materials and methods

2.1. Patients

Ten patients (five males, five females; age, 23–87 years; median age, 49.8 years) were included in this study. Pathological diagnosis was obtained by open surgery or stereotactic biopsy. Grading for the tumor was based on the World Health Organization grading system for neuroepithelial tumors [13]. Gradings for all participants in the study were as follows: pilocytic astrocytoma (Grade I), n=1; astrocytoma (Grade II), n=4; anaplastic astrocytoma (Grade III), n=1 and glioblastoma multiforme (GBM) (Grade IV), n=4. Written informed consent was obtained from all patients, and the study was approved by the institutional review board of the University of Fukui Hospital.

2.2. PET procedure

ACE and FDG PET were performed in all patients on separate days. PET scanning was undertaken using an Advance system (General Electric Medical Systems, Milwaukee, WI). The physical characteristics of this scanner have been described in detail by DeGrado et al. [14]. ACE was synthesized by carbonation of Grinaud's reagent followed by acid hydrolysis [15]. FDG was produced via the method of Hamacher et al. [16] using an automated FDG synthesis system. The specific activity was more than 50 GBq/μmol for ACE and 100–200 GBq/μmol for FDG. The radiochemical purity of both tracers was greater than 99%. Patients fasted at least 4 h before each PET examination. After obtaining a 10-min transmission scan with a ^{68}G rotating pin source, dynamic emission ACE PET scanning was performed for 20 min immediately following injection of 740 MBq of ACE, approximately. The ACE PET scan protocol was as follows: 1 min×10 frames and 5 min×2 frames. A 10-min FDG emission scan was performed 60 min postinjection of 185 MBq of FDG approximately, followed by postinjection transmission scanning for 10 min. Acquired emission data were reconstructed using the filtered back-projection method with a Hanning filter (6.5 mm). The reconstructed images were converted to standardized uptake value (SUV) images for the patient's body weight and injected dose.

2.3. Data analysis

For ACE PET, the static image obtained 10–20 min postinjection was used for data analysis as ACE uptake in cerebral cortex and glioma reached plateau after 10 min postinjection.

For visual assessment, both ACE and FDG PET images were compared with magnetic resonance (MR) images to determine tumor localization. The grading used for visual assessment was as follows: positive, tumor recognized as higher tracer uptake compared with normal cortex; negative, tumor recognized as lower tracer uptake compared with normal cortex and not detectable (ND), tumor unrecognized, with

Table 1
Patient characteristics and measured values

Sex/ age	Grade	CE on MRI	FDG			Acetate		
			Visual	SUV	T/C	Visual	SUV	T/C
Low grade								
F/28	I	Yes	Negative	6.41	0.66	ND	1.84	1.07
M/23	II	No	Negative	3.54	0.51	ND	1.07	0.96
F/36	II	Focal	Negative	4.72	0.67	Negative	1.82	0.89
F/36	II	No	Negative	5.48	0.55	ND	2.65	0.98
F/53	II	No	ND	3.42	0.72	Positive	1.87	1.77
Average				4.71	0.62		1.85	1.14
S.D.				1.28	0.09		0.56	0.36
High grade								
F/44	III	Focal	Positive	14.6	1.93	Positive	2.78	2.22
M/49	IV	Focal	ND	6.58	0.88	Positive	1.98	1.69
M/69	IV	Yes	ND	3.84	0.61	Positive	2.69	2.95
M/73	IV	Focal	Negative	5.12	0.63	Positive	2.63	2.34
M/87	IV	Focal	ND	5.48	0.84	Positive	3.05	2.63
Average				7.13	0.98		2.63	2.36
SD				4.31	0.55		0.46	0.63

CE, contrast enhancing; yes, homogeneous contrast enhancing; focal, spotty or ring-shaped contrast enhancing.

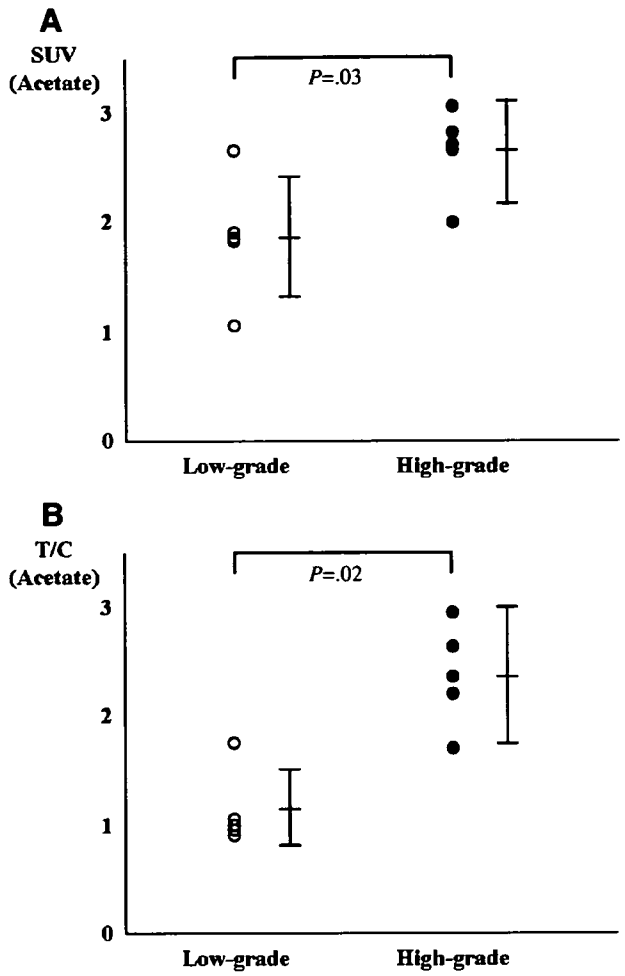

Fig. 2. Difference in SUV (a) and T/C (b) between low-grade and high-grade gliomas on ACE PET. Significant differences were observed for SUV (P=.03) and T/C (P=.02).

uptake almost equal compared to that of normal cortex. For quantitative assessment, regions of interest (ROIs) were placed on the tumor and contralateral cerebral cortex shown in Fig. 1. In this study, image coregistration between MR imaging (MRI) and PET was not performed, but by comparing MRI and PET images visually, ROIs were placed. As for the ROI placement on glioma with contrast-enhancing portion, ROIs were placed on the enhancing area while avoiding the nonenhancing area, which indicates necrosis. ROIs on the tumor were set to 8 mm in diameter because the largest-circle ROI that could avoid necrosis was 8 mm in diameter in our patient population. In glioma without a contrast-enhancing portion, T2-weighed images (T2WIs) were used as a guide to place ROI. In these patients, glioma showed high intensity compared to the cerebral cortex, but a very-high-intensity area, which indicates necrosis, was not found. Then, ROIs were placed on the center of the glioma. Irregular ROIs were placed to cover the cerebral cortex. Averaged SUV and tumor-to-cortex ratios (T/Cs) were then calculated. Because of the small number of patients, these data were compared between low-grade (Grades I and II) and high-grade (Grades III and IV) glioma.

2.4. Statistical analysis

Results are expressed as mean±S.D. Because of the small data set, nonparametric Mann–Whitney U test was applied to compare SUV and T/C between high-grade and low-grade glioma. SUV and T/C were compared for FDG and ACE using linear regression analysis. $P<.05$ was considered to be significant.

3. Results

Patient characteristics and measured values are summarized in Table 1. Two cases of low-grade glioma and all high-grade gliomas showed contrast enhancement on MRI.

In visual assessment, ACE PET findings were positive in all cases of high-grade glioma, although only one case was shown as positive on FDG PET. In contrast, four out of five cases of low-grade glioma were negative on FDG PET, while ACE PET could not detect the tumor in three of the five patients.

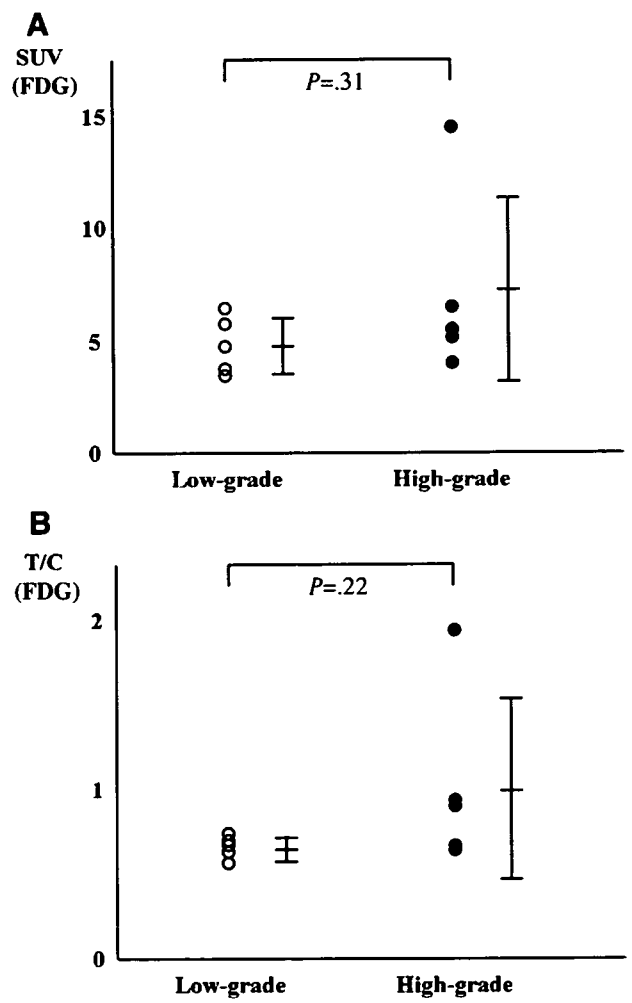

Fig. 3. Difference in SUV (a) and T/C (b) between low-grade and high-grade gliomas on FDG PET. No significant differences were observed for SUV (P=.31) and T/C (P=.22).

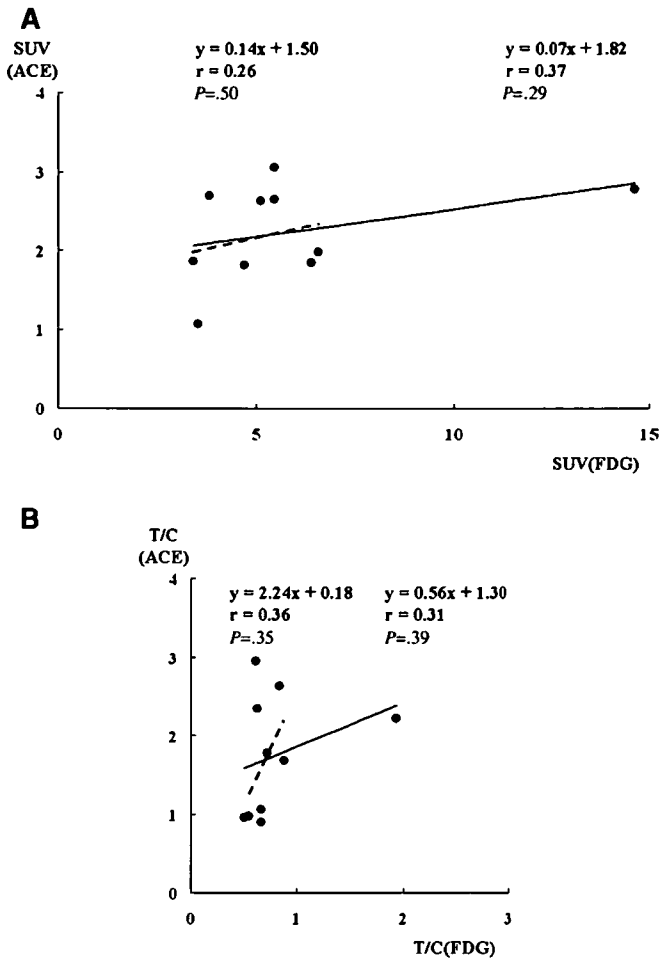

Fig. 4. Relationships of SUV (a) and T/C (b) between FDG and ACE. Regression lines with complete data set (solid line) and excluding outlier (dotted line) were demonstrated. No significant relationship was found (SUV, P=.29; T/C, P=.39), even excluding the outlier (SUV, P=.50; T/C, P=.35).

In terms of quantitative assessment, a significant difference was observed for SUV (2.63±0.46 vs. 1.85±0.56, P=.03) and T/C (2.36±0.63 vs. 1.14±0.36, P=.02) between low-grade and high-grade glioma on ACE PET, as shown in Fig. 2A and B, although no significant difference was observed for SUV (7.13±4.31 vs. 4.71±1.27, P=.31) or T/C (0.98±0.55 vs. 0.62±0.09, P=.22) on FDG PET, shown in Fig. 3A and B.

The relationship between FDG and ACE for SUV and T/C is shown in Fig. 4A and B. No significant relationship was observed (SUV, P=.29; T/C, P=.39), even excluding the outlier (SUV, P=.50; T/C, P=.35).

Representative cases of low-grade and high-grade glioma are shown in Figs. 5 and 6.

4. Discussion

In the present study, significant differences in SUV and T/C were observed on ACE PET, which means that ACE PET enables differentiation between low-grade and high-grade glioma. Regarding the mechanism of acetate uptake in the brain and in brain tumors, Dienel et al. [17] reported that acetate is preferentially transported into and metabolized by astrocytes and that the metabolism of acetate in glia-derived tumors includes the incorporation of radiolabeled substrates into acidic compounds and amino acids. They also reported the labeling of glial and meningeal tumors with 2-^{14}C-acetate; their in vitro study, using slices of human brain tumor, revealed that net uptake of 2-^{14}C-acetate was higher in high-grade glioma than in low-grade glioma.

In another in vitro study, Yoshimoto et al. [12] reported that the total and lipid-soluble fraction of ^{14}C metabolites from 1-^{14}C-acetate in five cell lines showed significant correlation with ^{3}H-methyl thymidine incorporation into DNA, which estimates growth activity. Our results are consistent with the findings of Dienel et al. [17] and are supported by the report of Yoshimoto et al. [12].

The results of the present study revealed a more significant difference in T/C compared with that of SUV on ACE PET, although both showed statistically significant differences between low-grade and high-grade glioma. Hustinx et al. [18] also reported that the measurement of activity ratio is superior to SUV for characterizing of primary brain tumor with FDG PET. We speculate that the reason for this result is as follows. ACE dynamic scanning in the report of Liu et al. [11] showed rapid uptake and clearance of ACE in the first 3 min followed by retention in the normal cortex. This may indicate that distribution of ACE in the normal cortex is affected by cerebral blood flow (CBF). It is well known that human aging causes CBF to decline [19,20]. In the present study, the mean age of the low-grade-glioma group was 35 years, while it was 64 years in the high-grade-glioma group. We consider that low CBF in the normal cortex causes a low retention of ACE; thus, a greater difference was observed in T/C. As for the aging effect on the brain tumor, the characteristic of brain tumor-like proliferative activity, which determines the degree of malignancy, is independent of the patient's age, that is, the decline of CBF does not necessarily mean the reduction of ACE uptake in brain tumors in elderly patients. Therefore, the decline of CBF is thought to be a main factor in causing a greater difference in T/C compared to SUV, although further examination using age-matched groups is required.

A statistical analysis revealed no significant relationship between FDG and ACE for either SUV or T/C. It is reported that acetate accumulation might be enhanced in gliomas by the transacceleration effect, which is stimulated by lactate efflux and may contribute to high tumor labeling with deoxyglucose [21,22]; however, our results did not support these data. Liu et al. [11] reported that 42% of 26 astrocytomas displayed discrepant uptake of ACE and FDG. Therefore, metabolic transacceleration is not a unique factor that can explain enhanced acetate uptake by astrocytomas; other factors must be further investigated.

In this study, two cases of low-grade glioma and all high-grade gliomas demonstrated contrast enhancement on MRI.

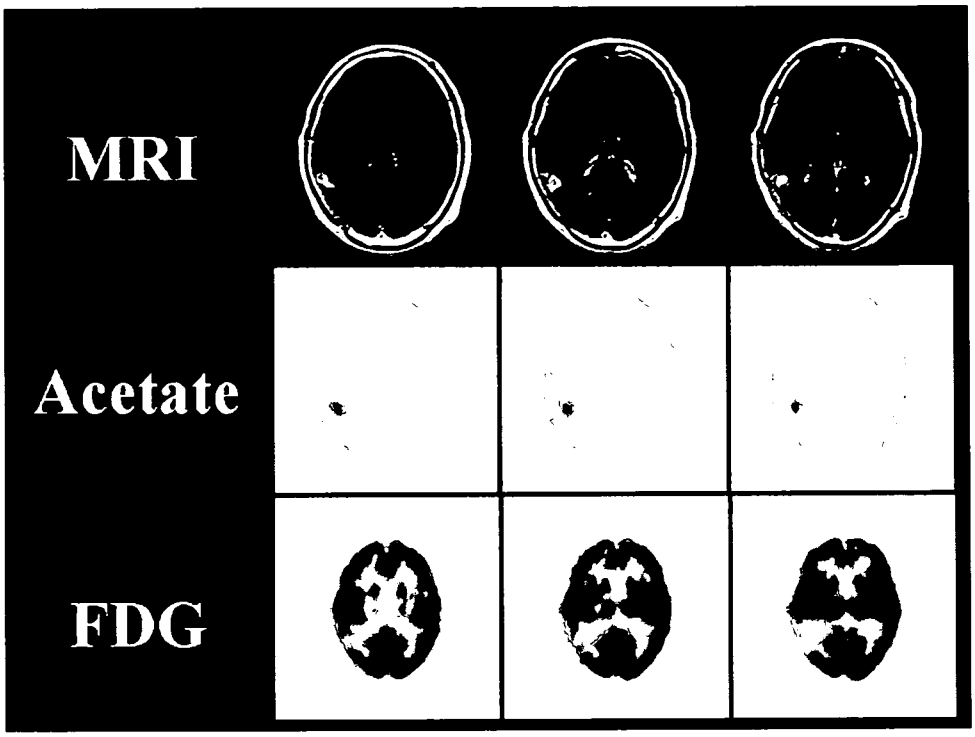

Fig. 5. MR images of a 69-year-old man diagnosed with GBM. The postcontrast T1-weighted images show contrast enhancement of the tumor in the right parietal lobe. Although ACE uptake was observed in the tumor (visual-positive), FDG uptake in the tumor was masked by cortical uptake of FDG (visual-ND).

Although contrast enhancement of a lesion is often taken as a sign of a high-grade lesion, low-grade glioma sometimes has an enhanced portion, as we experienced. Moreover, Ginsberg et al. [23] reported that the failure of gadolinium-enhanced MRI to visualize supratentorial brain tumors in adults does not indicate low-grade malignancy. These

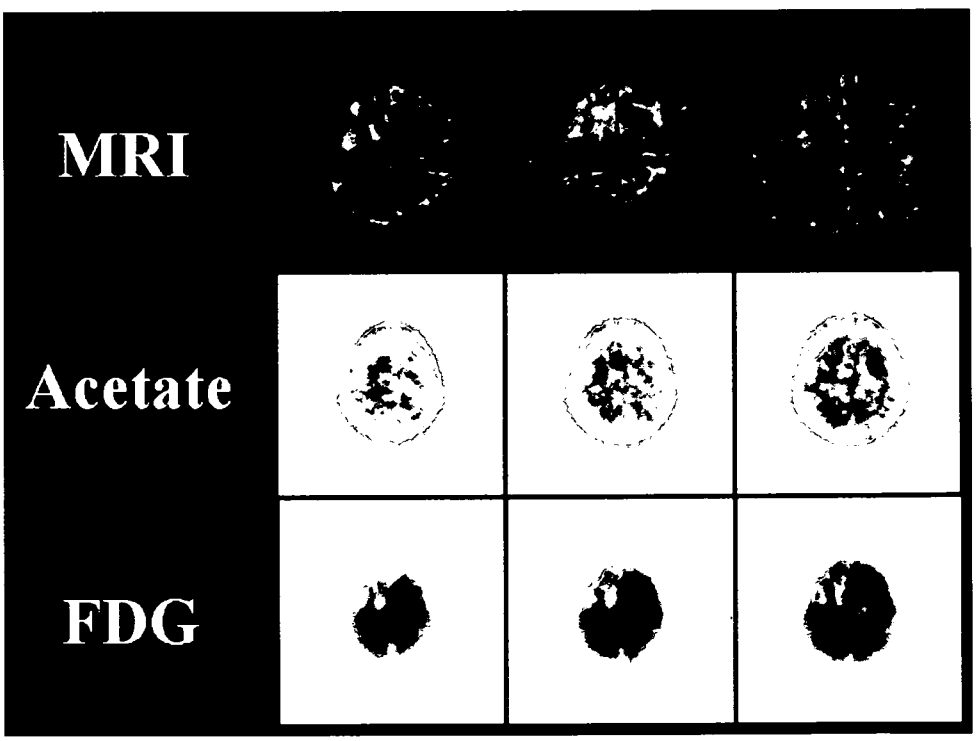

Fig. 6. MR images of a 36-year-old woman diagnosed with Grade II astrocytoma. An area of high intensity is demonstrated in the right frontal lobe on the T2WI. Although ACE uptake in glioma was not identified (visual-ND), less FDG uptake was observed in the glioma in comparison to cortical uptake (visual-negative).

indicate that applying contrast enhancement of the lesion has a limitation in determining the degree of malignancy, and a biological tracer like ACE, which reflects the growth activity directly, may be promising.

The fundamental limitation of the present study is the small number of patients. However, the fact that we have demonstrated the capability to differentiate between low-grade and high-grade glioma will be of value in encouraging further investigations using larger populations.

5. Conclusion

We evaluated the clinical significance of ACE PET findings for brain glioma, in comparison with FDG PET findings. ACE studies revealed a preliminary result of significant difference in SUV and T/C between low-grade and high-grade gliomas, indicating that ACE PET enables grading of brain glioma, although further confirmatory studies will be required.

References

[1] Gambhir SS, Czermin J, Schwimmer J, Silvermann DHS, Coleman RE, Phelps ME. A tabulated summary of the FDG PET literature. J Nucl Med 2001;42(Suppl):1S–71S.

[2] Coleman RE, Hoffman JM, Hanson MW, Sostman HD, Schold SC. Clinical application of PET for the evaluation of brain tumors. J Nucl Med 1991;32:616–22.

[3] DiChiro G. Positron emission tomography using [18F]fluorodeoxyglucose in brain tumors: a powerful diagnostic and prognostic tool. Invest Radiol 1986;22:360–71.

[4] Grosu AL, Piert M, Weber WA, Jeremic B, Picchio M, Schratzenstaller U, et al. Positron emission tomography for radiation treatment planning. Strahlenther Onkol 2005;181:483–99.

[5] Wong TZ, Westhuizen GJ, Coleman RE. Positron emission tomography imaging of brain tumors. Neuroimaging Clin N Am 2002;12: 615–26.

[6] Spence AM, Mankoff DA, Muzi M. Positron emission tomography imaging of brain tumors. Neuroimag Clin N Am 2003;13:717–39.

[7] Ogawa T, Inugami A, Hatazawa J, Kanno I, Murakami M, Yasui N, et al. Clinical positron emission tomography for brain tumors: comparison of fluorodeoxyglucose F-18 and L-methyl-^{11}C-methionine. AJNR Am J Neuroradiol 1996;17:345–53.

[8] Kaschten B, Stevenaert A, Sadzot B, Deprez M, Degueldre C, Del Fiore G, et al. Preoperative evaluation of 54 gliomas by PET with fluorine-18-fluorodeoxyglucose and/or carbon-11-methionine. J Nucl Med 1998;39:778–85.

[9] Sasaki M, Kuwabara Y, Yoshida T, Nakagawa M, Fukushima T, Mihara F, et al. A comparative study of thallium-201 SPET, carbon-11 methionine PET and fluorine-18 fluorodeoxyglucose PET for the differentiation of astrocytic tumours. Eur J Nucl Med 1998;25:1261–9.

[10] Ohtani T, Kurihara H, Ishiguchi S, Saito N, Oriuchi N, Inoue T, et al. Brain tumour imaging with carbon-11 choline: comparison with FDG PET and gadolinium-enhanced MR imaging. Eur J Nucl Med 2001;28: 1664–70.

[11] Liu RS, Chang CP, Chu LS, Chu YK, Hsieh HJ, Cahng CW, et al. PET imaging of brain astrocytoma with1-^{11}C acetate. Eur J Nucl Med Mol Imaging 2006;33:420–7.

[12] Yoshimoto M, Waki A, Yonekura Y, Sadato N, Murata T, Omata N, et al. Characterization of acetate metabolism in tumor cells in relation to cell proliferation: acetate metabolism in tumor cells. Nucl Med Biol 2001;28:114–22.

[13] Kleihues P, Burger PC, Scheithauer BW. Histological typing of tumors of the central nervous system. World Health Organization international classification of tumors. Berlin: Springer; 1993.

[14] DeGrado TR, Turkington TG, Willimas JJ, Stearns CW, Hoffman JM, Coleman RE. Performance characteristics of whole-body PET scanner. J Nucl Med 1994;35:1398–406.

[15] Kihlberg T, Valind S, Langstom B. Synthesis of [1-^{11}C], [2-^{11}C], [1-^{11}C](2H3) and [2-^{11}C](2H3) acetate for in vivo studies of myocardium using PET. Nucl Med Biol 1994;21:1067–72.

[16] Hamacher K, Coenen HH, Stocklin G. Efficient stereospecific synthesis of no-carried-added 2-[^{18}F]-fluoro-2-deoxy-D-glucose using aminopolyether supported nucleophilic substitution. J Nucl Med 1986;27:235–8.

[17] Dienel GA, Popp D, Drew PD, Ball K, Krisht A, Cruz NF. Preferential labeling of glial and meningial brain tumors with [2-14C]acetate. J Nucl Med 2001;42:1243–50.

[18] Hustinx R, Smith RJ, Benard F, Bhatnagar A, Alavi A. Can the standardized uptake value characterize primary brain tumors on FDG-PET? Eur J Nucl Med 1999;26:1501–9.

[19] Patano P, Baron JC, Lebrun-Grandie P, Duquesnoy N, Bousser MG, Comar D. Regional cerebral blood flow and oxygen consumptions in human aging. Stroke 1984;15:635–41.

[20] Martin AJ, Friston KJ, Colebatch JG, Frackowiak RS. Decrease in regional cerebral blood flow with normal aging. J Cereb Blood Flow Metab 1991;11:684–9.

[21] Greenberg HS, Chandler WF, Sandler HM. Brain tumors. New York: Oxford University Press; 1999. p. 58–77.

[22] Waniewski RA, Martin DL. Preferential utilization of acetate by astrocytes is attributable to transport. J Neurosci 1998;18:5225–33.

[23] Ginsberg LE, Fuller GN, Hashmi M, Leeds NE, Schomer DF. The significance of lack of MR contrast enhancement of supratentorial brain tumors in adults: histopathological evaluation of a series. Surg Neurol 1998;49:436–40.

資料(16)

Available online at www.sciencedirect.com
SCIENCE DIRECT
ELSEVIER
Nuclear Instruments and Methods in Physics Research A 563 (2006) 49–53
NUCLEAR INSTRUMENTS & METHODS IN PHYSICS RESEARCH Section A
www.elsevier.com/locate/nima

Studies of the performance of different front-end systems for flat-panel multi-anode PMTs with CsI(Tl) scintillator arrays

H. Sekiya[a,*], K. Hattori[a], H. Kubo[a], K. Miuchi[a], T. Nagayoshi[b], H. Nishimura[a], Y. Okada[a], R. Orito[c], A. Takada[a], A. Takeda[d], T. Tanimori[a], K. Ueno[a]

[a]*Department of Physics, Graduate School of Science, Kyoto University, Kitashirakawa, Sakyo, Kyoto 606-8502, Japan*
[b]*Advanced Research Institute for Science and Engineering, Waseda University, 17 Kikui-cho, Shinjuku, Tokyo 162-0044, Japan*
[c]*Department of Physics, Graduate School of Science and Technology, Kobe University, 1-1 Rokkoudai, Nada, Kobe 657-8501, Japan*
[d]*Kamioka Observatory, ICRR, University of Tokyo, 456 Higasi-mozumi, Hida-shi, Gifu 506-1205, Japan*

Available online 20 February 2006

Abstract

We have studied the performance of two different types of front-end systems for our gamma camera based on Hamamatsu H8500 (flat-panel 64 channels multi-anode PSPMT) with a CsI(Tl) scintillator array. The array consists of 64 pixels of $6 \times 6 \times 20\ mm^3$ which corresponds to the anode pixels of H8500.

One of the system is based on commercial ASIC chips in order to read out every anode. The others are based on resistive charge divider network between anodes to reduce readout channels. In both systems, each pixel (6 mm) was clearly resolved by flood field irradiation of ^{137}Cs. We also investigated the energy resolution of these systems and showed the performance of the cascade connection of resistive network between some PMTs for large area detectors.

PACS: 85.60.H; 87.62; 87.59; 95.55.K

Keywords: Flat-panel detector; PSPMT; Gamma camera; Compton telescope

1. Introduction

Recently, the concern with the gamma camera based on position-sensitive PMTs for application especially to nuclear medicine has been growing. The latest developed flat-panel-type Hamamatsu H8500 and H9500 [1] are promising devices for such purpose, and several studies have been conducted focusing on their spatial resolution with both pixellated scintillator array and continuous scintillator slab aiming at PET and SPECT applications [2–4].

The merit of such multi-anode flat-panel-type PMTs is the small non-active area when they are arrayed and constitute large area detectors, however, developments of readout systems for large number of channels are indispensable.

On the other hand, Compton imaging detectors for gamma ray astronomy or next generation medical imaging has been developed [5–7] with gamma cameras used for the detection of scattered gamma rays. In such cases, not only the spatial resolution but also the energy resolution is important to reconstruct the direction of incident gamma rays.

In this paper, we report the spatial resolution and energy resolution of our gamma camera based on H8500 with two different types of front-end systems. One of the system is based on commercial ASIC chips in order to read out every anode, the others are based on the resistive charge divider network between anodes to reduce the readout channels. In order to evaluate the performance, we coupled a CsI(Tl) scintillator array which fits to the anode pitches of H8500. This camera is intended for arrayed and covering our

*Corresponding author. Tel.: +81 75 753 3868; fax: +81 75 753 3799.
E-mail address: sekiya@cr.scphys.kyoto-u.ac.jp (H. Sekiya).

0168-9002/$ - see front matter © 2006 Elsevier B.V. All rights reserved.
doi:10.1016/j.nima.2006.01.096

micro-time projection chamber (micro-TPC) [5], which constitutes a new Compton imaging detector [8].

2. The detector

The Hamamatsu H8500 has a very compact dimension of 52 mm × 52 mm × 28 mm with 12 stages of metal channel dynodes and a HV divider circuit. The active photo cathode area is 49 mm × 49 mm and is covered by an 8 × 8 anode array. The typical anode gain is 10^6 (HV = −1000 V) and the typical anode gain uniformity (the ratio of the maximum gain to the minimum gain) is about 2.5. Each anode pixel size is 5.8 mm × 5.8 mm and the pitch between center of the anodes is 6.08 mm.

The size of each CsI(Tl) crystal is 6 mm × 6 mm × 20 mm. The crystals were also manufactured by Hamamatsu. Between the crystals, Vikuiti® ESR films (3M) of 65 μm are inserted for the optical isolation, so that the pixel of scintillator array corresponds to the anode pixel. The array is glued to H8500 using OKEN6262A optical grease. Fig. 1 shows the picture of the array.

3. Readout circuits

3.1. CP80068 system

Fig. 2 shows the individual anode readout system (Clear Pulse Co., Ltd. CP80068). The dimension of CP80068 which is designed for two-dimensional array of H8500 is 52 mm × 52 mm × 95 mm. It is based on two types of analog ASICs, VA32HDR14 and TA32CG2 manufactured by IDEAS ASA. VA32HDR14 contains pre-amplifiers (input dynamic range ~ ± 15 pC), shapers (gain = 118 mV/pC, peaking time = 2 μs), sample and hold circuits and a multiplexer. TA32CG32 contains fast shapers (peaking time = 75 ns) and comparators, which can make the trigger signals. The multiplexed 64 ch data are digitized by a flash ADC on the CP80068 and sent to the VME sequence module via FPGAs. It takes 164 μs to process one event (64 channels).

3.2. Resistive charge division

Fig. 3 shows the charge divider network board for H8500. Using this connector board, the anodes in

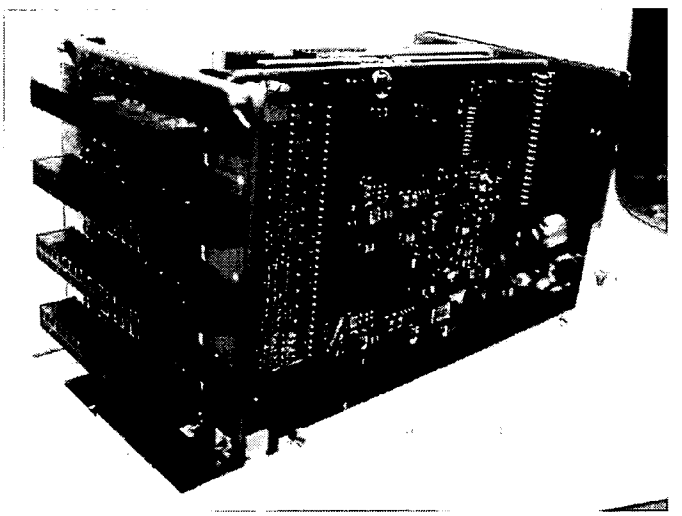

Fig. 2. Picture of CP80068.

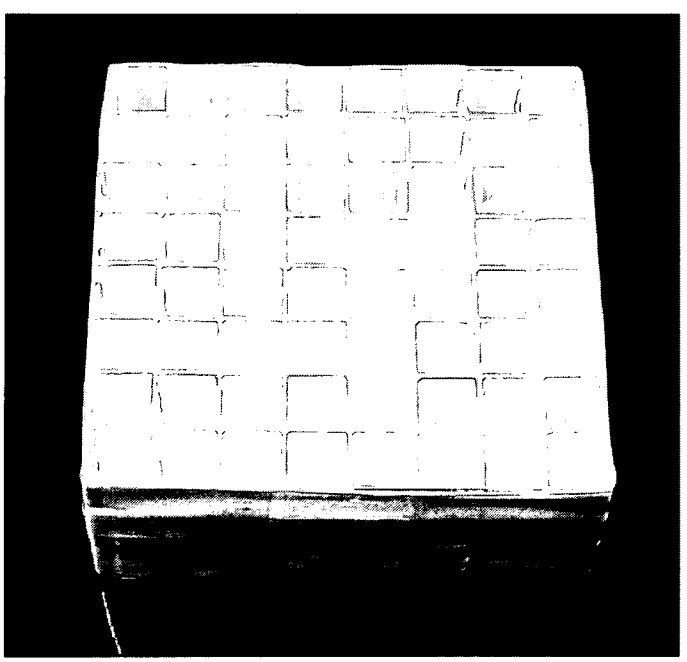

Fig. 1. Picture of the CsI(Tl) array.

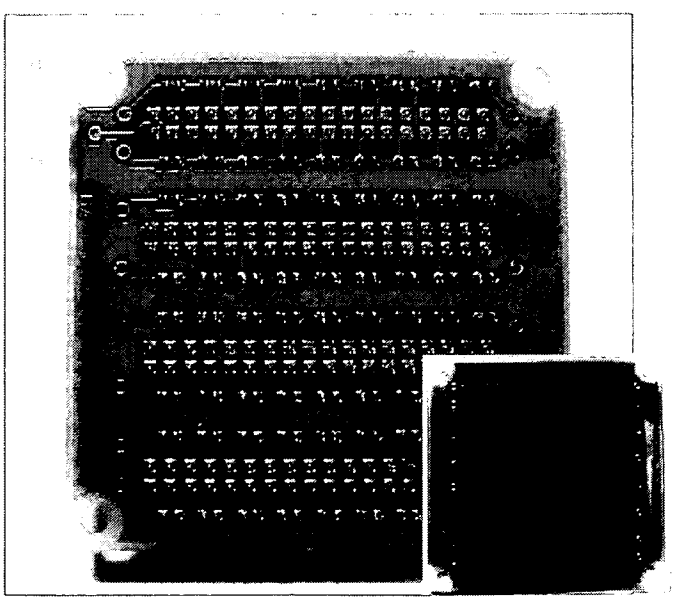

Fig. 3. Bottom view of the resistive divider network for H8500 and the top view (inset).

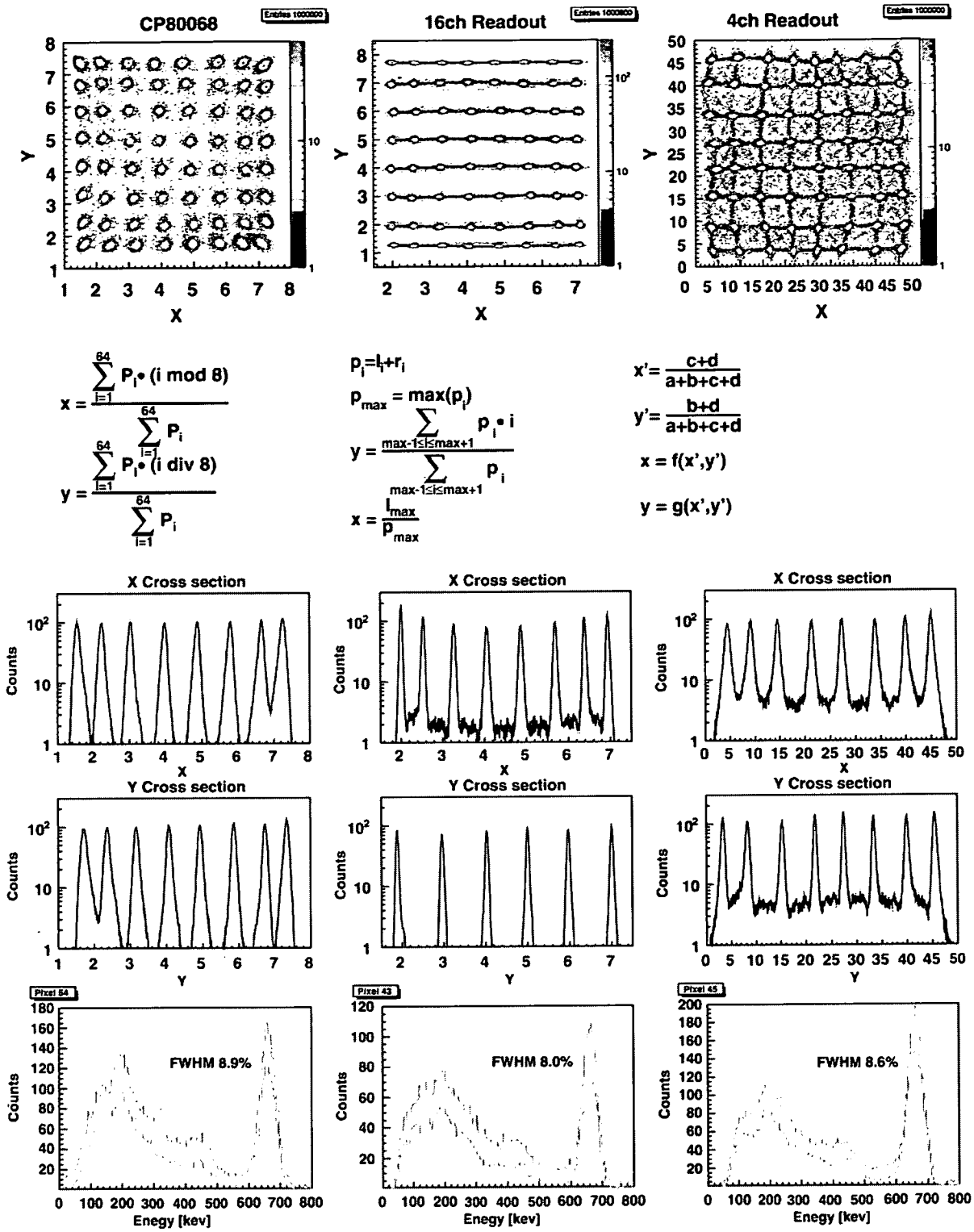

Fig. 4. Measurement results of each readout system. Flood field images of ^{137}Cs irradiation, methods of the position reconstruction, x and y cross-sections of central rows, the energy spectra of the best pixel of every readout system are shown. In the equations, P_i is the ADC output of ith anode of CP80068 system, $l_i(r_i)$ is the ADC output of left (right) side of ith horizontal resistive chain of 16 channels readout system, $a \cdot b \cdot c \cdot d$ represent the ADC outputs of four terminals of four channels readout system. In four channels readout system, as the raw image (x', y') is distorted, the corrected image (x, y) calculated by TMultiDimFit class of ROOT [9] is indicated.

horizontal rows of H8500 are connected with 100 Ω chips and the number of readout channels are reduced to 16. Each reduced channel is preamplified (integrating time constant = 66 μs), shaped (Clear Pulse CP4026, shaping time = 2 μs) and digitized (CAEN V785). The last dynode output is used as the trigger signal.